

# Dynamics of the modulation instability spectrum in optical fibers with oscillating dispersion

M. Droques, A. Kudlinski,\* G. Bouwmans, G. Martinelli, and A. Mussot  
*Université Lille 1, Laboratoire PhLAM, IRCICA, 59655 Villeneuve d'Ascq, France*

(Received 17 October 2012; published 15 January 2013)

A simple analytical model is developed to analyze and explain the complex dynamics of the multi-peak modulation instability spectrum observed in dispersion oscillating optical fibers [M. Droques *et al.*, *Opt. Lett.* **37**, 4832 (2012)]. We provide a simple expression for the local parametric gain, which shows that each of the multiple spectral components grows thanks to a quasi-phase-matching mechanism due to the periodicity of the waveguide parameters, in good agreement with numerical simulations and experiments. This simplified model is also successfully used to tailor the multi-peak modulation instability spectrum shape. These theoretical predictions are confirmed by experiments.

DOI: [10.1103/PhysRevA.87.013813](https://doi.org/10.1103/PhysRevA.87.013813)

PACS number(s): 42.65.Ky, 42.65.Tg, 42.65.Wi, 42.65.Hw

## I. INTRODUCTION

Modulation instability (MI) is a nonlinear process in which a weak perturbation is exponentially amplified by an intense field. MI has been investigated in many sub-fields of physics, especially in optics, for which experiments in both homogeneous and periodic media are relatively simple [1]. The additional degree of freedom brought by the periodicity has caught the attention of many research groups and has led to many theoretical and experimental works in spatial [2,3] and temporal Kerr media such as optical fibers [4–7]. This physical flexibility is of particular interest since the modulation period can be varied from the meter range up to tens of kilometers, leading to a broad range of investigation. In the 1990s the rise of optical telecommunication networks led to the deployment of “natural” periodic optical fiber systems due to the alternation of all-optical regeneration devices and/or dispersion managed lines [8,9]. In addition to the fundamental interest brought by these systems, it was then necessary to understand in depth the origin of the characteristic spurious MI sidebands [8,9], which are highly detrimental to telecommunications since they are generated in the gigahertz range [6,7] due to their period in the range of kilometers. Many theoretical studies have therefore been initiated in this context [6,8–15].

Very recently, dispersion management was pushed one step further with the experimental demonstration of MI in continuously modulated waveguides [16,17]. From these results, the spurious consequence of the MI sidebands due to the periodicity can be turned into a benefit since these works show the possibility to obtain multiple parametric gain bands in the terahertz range. It should then provide another degree of freedom for designing optical systems requiring broad bandwidths such as in all-optical signal processing systems where there is a growing demand.

While a deep theoretical study of MI in periodically tapered fibers has been reported very recently [18], we propose in the present work a simplified analytical treatment allowing an accurate description of the MI dynamics and the tailoring of the overall shape of its multi-peak spectrum. Besides providing insight into the underlying physics, our analytical treatment allows us to derive an expression for the local linear parametric

gain. Finally, in order to illustrate the practical interest of this simple analysis, we report experiments in which the multi-peak MI spectrum has been tailored to suppress one MI sideband or to favor a single strong one, in good agreement with our analytical predictions.

## II. CONTEXT

We recently reported the experimental demonstration of MI in a dispersion oscillating fiber (DOF) [17]. Although details can be found in Ref. [17], the aim of this section is to briefly summarize our previous results in order to facilitate the reading of the present paper. Figure 1 shows a measurement of the evolution of the fiber diameter along its length. The outer diameter follows a sine shape with a modulation amplitude of  $\pm 7\%$  and a period  $Z$  of 10 m, which results in a dispersion modulation over the fiber length  $z$  with a quasi-sinusoidal shape over the wavelength range of interest here, written as

$$\beta_2(z) = \overline{\beta}_2 + \beta_2^A \sin\left(\frac{2\pi z}{Z}\right), \quad (1)$$

where  $\overline{\beta}_2 = 1.2 \times 10^{-27} \text{ s}^2/\text{m}$  is the average second-order dispersion and  $\beta_2^A = 1.5 \times 10^{-27} \text{ s}^2/\text{m}$  is the amplitude modulation at our pump wavelength of 1072 nm.

Solid circles in Fig. 1(b) correspond to the spontaneous MI spectrum obtained by pumping a 120-m-long sample of this DOF (which we call DOF1) with 2-ns pulses with a peak power  $P_p$  of 20 W at  $\lambda_p = 1072 \text{ nm}$ . The solid line represents the spectrum resulting from the numerical integration of the generalized nonlinear Schrödinger equation (GNLSE) seeded by noise to accurately reproduce experimental random initial conditions (all details and parameters are given in Ref. [17]). Both spectra are in good agreement (except for the higher experimental noise floor) and show the generation of multiple MI sidebands pairs [19] spanning over more than 10 THz. The frequency of these parametric sidebands can be roughly estimated from a quasi-phase-matching relation developed in the case of an infinitely long grating [6,8,9]

$$\overline{\beta}_2 \Omega_k^2 + 2\gamma P_p = 2\pi k/Z, \quad (2)$$

where  $k$  is an integer,  $\Omega_k$  is the pulsation detuning from the pump, and  $\gamma$  is the average nonlinear coefficient of the DOF.

\*alexandre.kudlinski@univ-lille1.fr

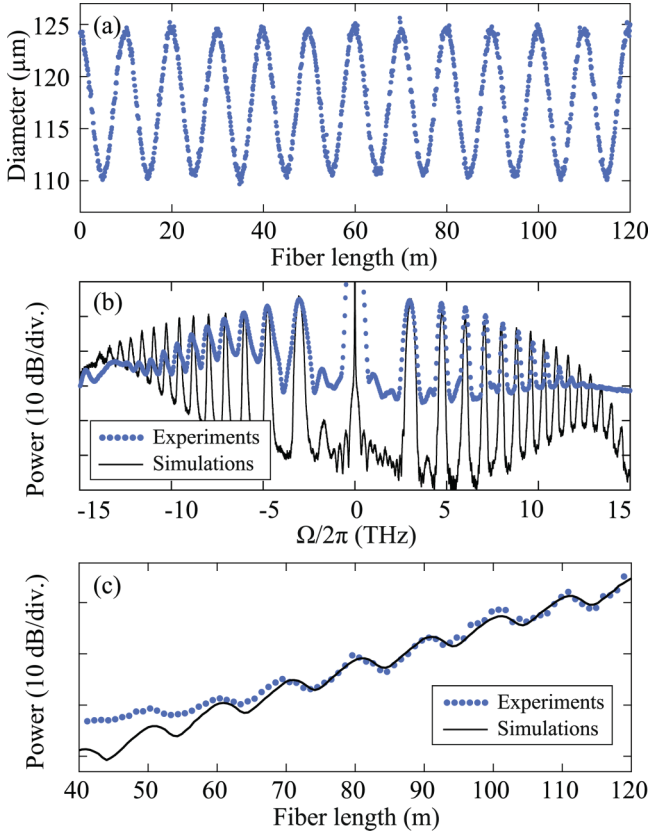


FIG. 1. (Color online) (a) Outer diameter of the DOF versus fiber length measured during fiber drawing. (b) Experimental (circles) and simulated (solid line) spectra obtained for a pump power of 20 W and a fiber length of 120 m. (c) Evolution of the power of the first sideband ( $k = 1$ ) versus fiber length obtained from experiments (circles) and numerical simulations (solid line). Results are from Ref. [17].

The dynamics of the MI process with fiber length was investigated by cutting back the DOF and recording output spectra. As an illustration, Fig. 1(c) shows the evolution of the power of the first sideband ( $k = 1$ ) versus fiber length obtained from experiments (circles) and numerical simulations (solid line). The dynamics observed in both experiments and simulations exhibits periodic regions of deamplification, which makes the side lobe power oscillate along the fiber around the exponential growth (expected for a perfectly phase-matched process). Such a dynamics is expected from quasi-phase-matched processes, but it differs from the one observed in second-order nonlinear crystals in which there are no regions of deamplification. This particular and unusual feature will now be studied in detail with the help of a simple and intuitive analytical model in order to provide further insight into the underlying physics.

### III. ANALYTICAL MODEL

#### A. Parametric gain calculation

It is well established that the MI process can be interpreted in the spectral domain as a four-wave mixing (FWM) process [24,25]. In this frame, the parametric FWM gain spectrum can be obtained by studying the stability of the steady state

solution against weak perturbations through a so-called linear stability analysis. In dispersion managed optical systems, this tool has allowed the analytical prediction of the complex multi-peak gain spectrum [9,11], but such an analysis does not provide any clear insight into the dynamics of the process nor any details about the fine evolution of the field over a single modulation period of the fiber. To this aim, we propose here a more intuitive explanation of the results from Ref. [17] by revisiting a simplified truncated three-wave model usually aimed at describing Fermi-Pasta-Ulam recurrence and fiber-optic parametric amplification [26–28]. This model allows one to account for the relative phase variations between pump, signal, and idler waves during propagation. In our work, it will be induced by the longitudinal variations of dispersion rather than pump depletion. Our starting point is the four coupled differential equations given by Eqs. (3) in Ref. [27]. We neglect fiber loss and assume that the pump remains undepleted and that signal and idler powers  $P_s$  and  $P_i$  are much less than the pump power  $P_p$  over the whole DOF length. It is then easy to show that this system reduces to the equations

$$\begin{aligned} \frac{dP_s(\Omega, z)}{dz} &= 2\gamma P_p \sqrt{P_s(\Omega, z)P_i(\Omega, z)} \sin\theta(\Omega, z), & (3a) \\ \frac{dP_i(\Omega, z)}{dz} &= 2\gamma P_p \sqrt{P_i(\Omega, z)P_s(\Omega, z)} \sin\theta(\Omega, z), & (3b) \\ \frac{d\theta(\Omega, z)}{dz} &= \Omega^2 \left[ \bar{\beta}_2 + \beta_2^A \sin\left(\frac{2\pi z}{Z}\right) \right] \\ &\quad + 2\gamma P_p \{1 + \cos[\theta(\Omega, z)]\}, & (3c) \end{aligned}$$

where  $\Omega$  is the shift of the signal and idler pulsations from the pump and  $\theta(\Omega, z)$  describes the longitudinal evolution of the relative phase difference between all these waves [27]. The discrepancy between solutions of Eq. (2) and experimental or numerical values mentioned in Ref. [17] can now be understood from Eq. (3c). Indeed, Eq. (2) assumes that the nonlinear phase mismatch can be approximated by  $2\gamma P_p$  [6,8,9], while Eq. (3c) shows that it is in fact equal to  $2\gamma P_p \{1 + \cos[\theta(\Omega, z)]\}$ . This does not impact the validity of the present results since this additional term remains low for the pump powers involved in the present study. In order to obtain a simple analytic solution of the set of equations (3), we thus neglect the last term  $\cos[\theta(\Omega, z)]$  in Eq. (3c). This physically means that we assume that the longitudinal evolution of the nonlinear phase mismatch term is weak compared to the linear and uniform nonlinear phase mismatch terms, which is valid for low pump powers. By integrating the set of equations (3), we find that the total accumulated gain of the signal in power is written as

$$\begin{aligned} G(\Omega, z) &= \frac{P_s(\Omega, z)}{P_s(\Omega, 0)} = \frac{1}{4} [1 - \rho] \\ &\quad + \frac{1}{4} [1 + \rho + 2\sqrt{\rho}] \exp \left[ \int_0^z g(\Omega, z') dz' \right], & (4) \end{aligned}$$

with  $\rho = P_i(\Omega, 0)/P_s(\Omega, 0)$ . In the following, we set  $\rho = 1$  for the sake of simplicity. In Eq. (4),  $g(\Omega, z) = 2\gamma P_p \sin[\theta(\Omega, z)]$  is the local linear gain. Its calculation requires integrating Eq. (3c) in order to evaluate  $\theta(\Omega, z)$ , which gives (under our

assumptions)

$$\theta(\Omega, z) = [\overline{\beta_2} \Omega^2 + 2\gamma P_p]z + \frac{\beta_2^A \Omega^2}{2\pi/Z} [1 - \cos(2\pi z/Z)] + \theta(\Omega, 0). \quad (5)$$

Finally, by using a Fourier series expansion to calculate the  $\sin[\theta(\Omega, z)]$  term, we find that the local linear gain is written as

$$g(\Omega, z) = 2\gamma P_p \sum_{q=-\infty}^{q=+\infty} J_q \left( \frac{\beta_2^A \Omega^2}{2\pi/Z} \right) \times \sin \left[ \left( \overline{\beta_2} \Omega^2 + 2\gamma P_p - \frac{q2\pi}{Z} \right) z + K_q \right], \quad (6)$$

with  $K_q = \frac{\beta_2^A \Omega^2}{2\pi/Z} - q\frac{\pi}{2} + \theta(\Omega, 0)$ . Thus Eq. (6) indicates that the linear gain  $g(\Omega, z)$  at a fixed pulsation detuning  $\Omega$  can be interpreted as the sum of sine functions in  $z$ . These sine functions all have a zero average value except when their argument becomes independent of  $z$ . It only occurs at specific spectral components  $\Omega$  [equal to the pulsation  $\Omega_k$  in Eq. (2)] corresponding to solutions of the quasi-phase-matching relation (2). For these specific pulsation detunings  $\Omega_k$ , each term of the sum in Eq. (6) leads to periodic amplification and deamplification phases along the DOF except for the uniform contribution corresponding to  $q = k$ . This last term therefore prevails over the other ones on the gain  $G(\Omega, z)$  for long enough propagation distances. Thus the linear gain of the  $k$ th spectral component mainly depends on this uniform term as long as the fiber exceeds a few modulation periods. It is then equal to  $2\gamma P_p |J_k(\frac{\beta_2^A \Omega_k^2}{2\pi/Z})|$  by choosing  $K_k = \frac{\pi}{2}$  as initial condition. Note that this is analogous to the choice of maximizing the gain in MI in uniform fibers by setting the initial phase mismatch value to  $\pi/2$  [27,28].

### B. Physical interpretation

To illustrate this process, we first focus on the first spectral component ( $k = 1$ ). The solid black line in Fig. 2(a) shows the evolution of the maximum gain (at  $\Omega = \Omega_{\max}^{\text{simu}}$ ) obtained from numerical integration of the complete set of original equations (3). Note that an excellent agreement is achieved with the numerical integration of the GNLS (not shown here for the sake of clarity). The blue solid line in Fig. 2(a) corresponds to the term of uniform gain (Bessel function  $J_1$ ), the blue dotted and dashed lines correspond to the highest amplitude oscillating terms (Bessel functions  $J_0$  and  $J_{-1}$ , respectively, in this case), and the red solid line corresponds to their sum. We limit our investigations to  $J_0$  and  $J_{-1}$  because all other Bessel functions have much lower contributions in this example. A good agreement is obtained between the red solid curve from the analytical model and the black one from numerical simulations, which confirms the validity of our assumptions and the accuracy of our method. In each modulation period, the amplification phase is characterized by  $0 < \theta(\Omega, z) < \pi$  and the deamplification one has  $-\pi < \theta(\Omega, z) < 0$ , as represented in Fig. 2(b), the total phase shift being equal to  $2\pi$  per period.

The dynamics of the second spectral component ( $k = 2$ ) is shown in Fig. 3. The same reasoning as for the first one ( $k = 1$ ) can be applied. The  $J_2$  term provides the average

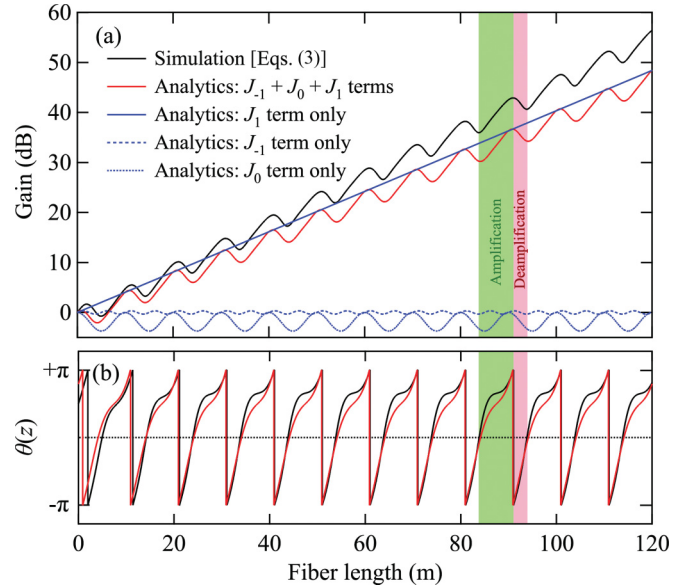


FIG. 2. (Color online) (a) Evolution of the gain of the first amplified frequency ( $k = 1$ ) from Eq. (4), with the contribution of  $J_1 + J_0 + J_{-1}$  (average gain plus oscillating terms) (solid red line), for  $J_1$  only (blue solid line), for  $J_0$  only (blue dotted line), and for  $J_{-1}$  only (blue dashed line) with  $\Omega_{\max}^{\text{theo}} = 2\pi \times 2.63 \times 10^{12}$  rad/s [Eq. (2)]. The solid black line is calculated from the numerical integration of the original set of equations [Eqs. (3)] with  $\Omega_{\max}^{\text{simu}} = 2\pi \times 2.93 \times 10^{12}$  rad/s. (b) Evolution of  $\theta(z)$  from our analytical study (solid red line) and from numerical simulations with Eqs. (3) (solid black line). The green area corresponds to amplification and the red one to deamplification over one period.

exponential gain (blue solid line) and additional oscillating terms provide the oscillating behavior of the overall gain. By taking the five terms with highest amplitude into account (from  $k = -2$  to 2), good agreement between Eq. (4) and numerical simulations from Eqs. (3) is achieved. Note that adding other higher-order terms does not significantly change the analytical results (displayed as red curves). For the sake of clarity, only the two highest amplitude terms ( $J_{-1}$  and  $J_1$ ) are represented in Fig. 3(a) (as dashed and dotted lines, respectively). In this case, there are two amplification and deamplification phases per period. The evolution of the phase represented in Fig. 3(b) also shows a more complex evolution than for the first ( $k = 1$ ) sideband and the total phase shift is now equal to  $4\pi$  per period. The agreement between numerical simulations from Eqs. (3) (black lines) and our analytical result (red lines) is excellent for the evolution of both the gain and the phase.

Figures 2 and 3 emphasize that the dispersion modulation enables one to control the evolution of the relative phase of the waves so that the whole process can be seen as quasi-phase-matched, the variation of the relative phase over one period being equal to  $2k\pi$  for the  $k$ th spectral component. Indeed, this relative phase  $\theta(\Omega, z)$  would grow linearly in the absence of the modulation term ( $\beta_2^A = 0$ ) in Eq. (3c) [29]. This linear growth would lead to amplification and deamplification phases of the same length and consequently the total accumulated gain would be negligible.

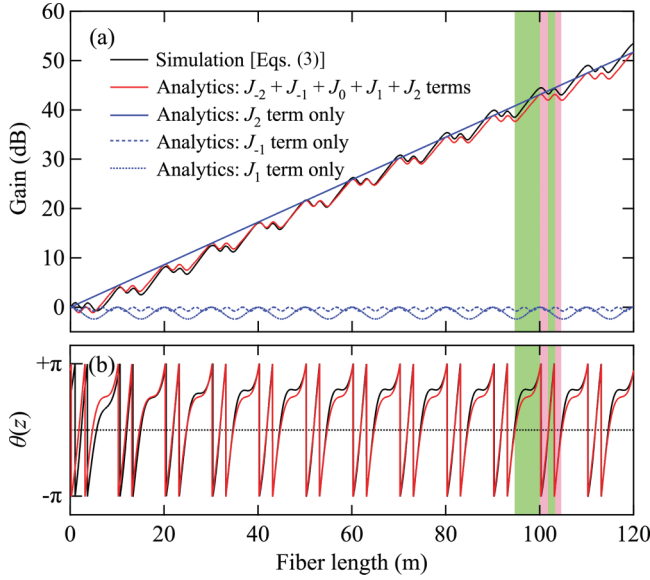


FIG. 3. (Color online) (a) Evolution of the gain of the second amplified frequency ( $k = 2$ ) from Eq. (4), with the contribution of  $J_{-2} + J_{-1} + J_0 + J_1 + J_2$  (average gain plus oscillating terms) (red solid line), for  $J_2$  only (blue solid line), for  $J_1$  only (blue dotted line), and for  $J_{-1}$  only (blue dashed line) with  $\Omega_{\max}^{\text{theo}} = 2\pi \times 4.49 \times 10^{12}$  rad/s [Eq. (2)]. The solid black line is calculated from the numerical integration of the original set of equations [Eqs. (3)] with  $\Omega_{\max}^{\text{simu}} = 2\pi \times 4.61 \times 10^{12}$  rad/s. (b) Evolution of  $\theta(z)$  from our analytical study (solid red line) and from numerical simulations with Eqs. (3) (solid black line). Green areas correspond to amplification and the red ones to deamplification over one period.

From a more practical point of view, the frequency of the spectral component  $\Omega_k$  can be widely modified simply by changing the periodicity of the grating (as in a diffraction grating for the position of its different orders), while the gain (analogous to the diffraction efficiency in a specific order) can be modulated independently through the ratio  $\beta_2^A/\beta_2$ . Note, however, that the deamplification phases of the signal along the fiber cannot be totally avoided, only reduced. This can be understood either by considering that they are due to the contribution of all oscillating terms of Eq. (6), which cannot all be suppressed simultaneously, or by considering that the dispersion grating enables the evolution of  $\theta(\Omega, z)$  to deviate from a linear growth but not to limit its evolution in the  $[0; \pi]$  range required for a positive gain [see Eq. (3a)].

#### IV. EVOLUTION OF THE MI SPECTRUM WITH AVERAGE DISPERSION

In order to further emphasize the accuracy of our simplified analytical model, we studied the evolution of the MI spectrum as a function of the average dispersion value at the pump frequency in both normal and anomalous dispersion regimes. We chose the DOF parameters so that they would match the ones of the fiber used hereafter. We took into account longitudinal variations of  $\beta_2$  according to Eq. (1) and average values of  $\gamma$ ,  $\beta_3$ , and  $\beta_4$  instead of their longitudinal evolution. We checked numerically that this would have negligible impact in our conditions. The DOF parameters are  $\beta_2^A$  of  $10^{-27}$  s<sup>2</sup>/m,  $\beta_3 = 6.8 \times 10^{-41}$  s<sup>3</sup>/m,  $\beta_4 = 1.7 \times 10^{-55}$  s<sup>4</sup>/m,

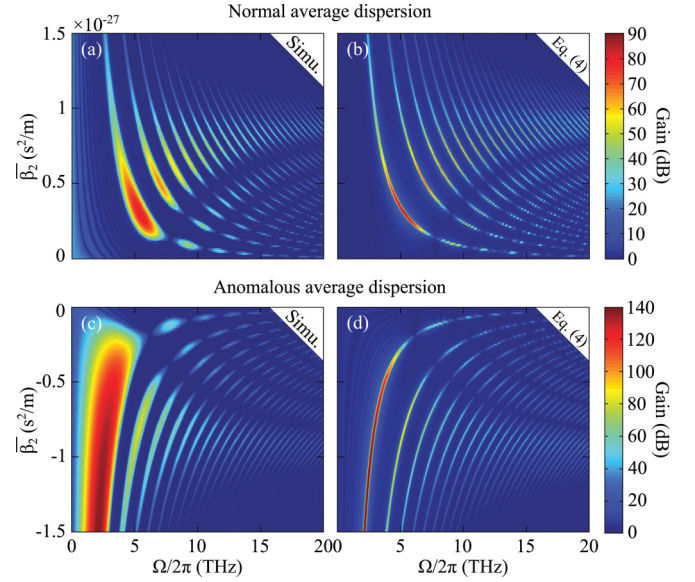


FIG. 4. (Color online) Top view of the gain spectrum (on a logarithmic scale) obtained from (a) and (c) GNLSE simulations and (b) and (d) our analytical model [Eq. (4)] as a function of the average second-order dispersion. (a) and (b) correspond to average normal dispersion pumping and (c) and (d) to anomalous average dispersion pumping. The zero frequency corresponds to the pump.

and  $\gamma = 7$  W<sup>-1</sup> km<sup>-1</sup> at 1064 nm. The DOF is 120 m long and the modulation period is  $Z = 10$  m. Fiber attenuation and stimulated Raman scattering are neglected.

We first performed numerical simulations using Eq. (4) by varying values of  $\beta_2$  from  $-1.5$  to  $1.5 \times 10^{-27}$  s<sup>2</sup>/m. The maps displayed in Figs. 4(a) and 4(c) represent calculated numerical gain spectra (on a logarithmic scale) for varying  $\beta_2$  values in normal and anomalous dispersion regions, respectively. For the sake of clarity, only one half of the overall spectrum is displayed, the other half being perfectly symmetric with respect to the pump frequency. In parallel, we have plotted in Figs. 4(b) and 4(d) the same maps using the analytical gain expression given by Eq. (4) with the same parameters as for the numerical simulations. There is a good qualitative agreement between both graphs, although quantitative agreement is not reached due to our approximations explained above. However, our model allows us to reproduce the specific dynamical features observed in numerical simulations.

First, the detuning of each MI sideband from the pump decreases as  $\beta_2$  increases, as expected from Eq. (2).

Second, the gain strongly depends on  $\beta_2$ , which differs from classical MI spectrum observed in uniform fibers in the anomalous dispersion regime, in which the maximal parametric gain does not depend on  $\beta_2$ . Additionally, the maximal gain does not correspond to the same  $\beta_2$  value for each MI sideband.

Third, we can identify specific  $\beta_2$  values for which one or several initially well-defined MI sideband are canceled, i.e., their parametric gain vanishes. The frequency of canceled sidebands increases with increasing  $\beta_2$  values for each value of  $k$ . This *a priori* unexpected cancellation of parametric gain

is in fact due to vanishing  $J_k$  functions in Eq. (6) and will be detailed in Sec. V A.

### V. TAILORING THE MI GAIN SPECTRUM

The simple analytical approach presented in Sec. III and further confirmed in Sec. IV allows a better understanding of the complex dynamics of the process and has allowed us to design experiments in which the multi-peak gain spectrum is tailored. To illustrate this, we focus our attention here on two striking examples. We chose either to completely cancel a given spectral component (as previously mentioned in Sec. IV) or to maximize the gain of a sideband pair with regard to the others. To reach these goals, let us recall that, as detailed in the analytical model above, the linear gain of the  $k$ th spectral component can be approximated by

$$\begin{aligned} g(\Omega_k, z) &= 2\gamma P_p \left| J_k \left( \frac{\beta_2^A \Omega_k^2}{2\pi/Z} \right) \right| \\ &= 2\gamma P_p \left| J_k \left[ \frac{\beta_2^A}{\beta_2} \left( k - \frac{\gamma P_p Z}{\pi} \right) \right] \right|. \end{aligned} \quad (7)$$

Equation (7) indicates that the gain of the  $k$ th spectral component can be totally canceled by simply finding the argument

$$\eta = \frac{\beta_2^A \Omega_k^2}{2\pi/Z} = \frac{\beta_2^A}{\beta_2} \left( k - \frac{\gamma P_p Z}{\pi} \right)$$

for which the Bessel function  $J_k$  vanishes. Here  $\eta$  can be adjusted by controlling the modulation amplitude of dispersion  $\beta_2^A$  or the fiber period  $Z$ , which both require manufacturing new DOF samples. However, it can also be adjusted by controlling the average dispersion at the pump wavelength  $\bar{\beta}_2$ , which can be done experimentally by simply tuning the pump wavelength.

#### A. Cancellation of the spectral component

To illustrate this, we fabricated a new DOF sample, referred to as DOF2 hereafter. The DOF2 sample is 120 m long and has an average dispersion  $\bar{\beta}_2$  of  $10^{-27}$  s<sup>2</sup>/m and a modulation amplitude  $\beta_2^A$  of  $10^{-27}$  s<sup>2</sup>/m at 1064 nm; its zero-dispersion wavelength oscillates between 1064 and 1080 nm. The average third-order dispersion term is  $\beta_3 = 6.8 \times 10^{-41}$  s<sup>3</sup>/m, the average nonlinear coefficient is  $\gamma = 7$  W<sup>-1</sup> km<sup>-1</sup>, and the attenuation is  $\alpha = 7.5$  dB/km at 1064 nm. To illustrate the cancellation of parametric gain at specific frequencies, we choose to cancel, for example, the  $k = 6$  sideband pair. In this case, we find that  $J_6$  vanishes for a  $\bar{\beta}_2$  of  $5.8 \times 10^{-28}$  s<sup>2</sup>/m with the parameters of DOF2 given above and a pump power of 13 W. Circles in Fig. 5(a) show the gain calculated with the above model [Eq. (7)] for each spectral component and for a fiber length of 120 m, while the solid line represents the output spectrum obtained from a numerical integration of the GNLSE with a pump power of 13 W. We average 50 output spectra seeded by random initial conditions to account for the averaging performed during the experimental recording of a spectrum. These results confirm the ability of our simplified model to correctly predict the maximal gain of each sideband and also show that the  $k = 6$  spectral component is indeed

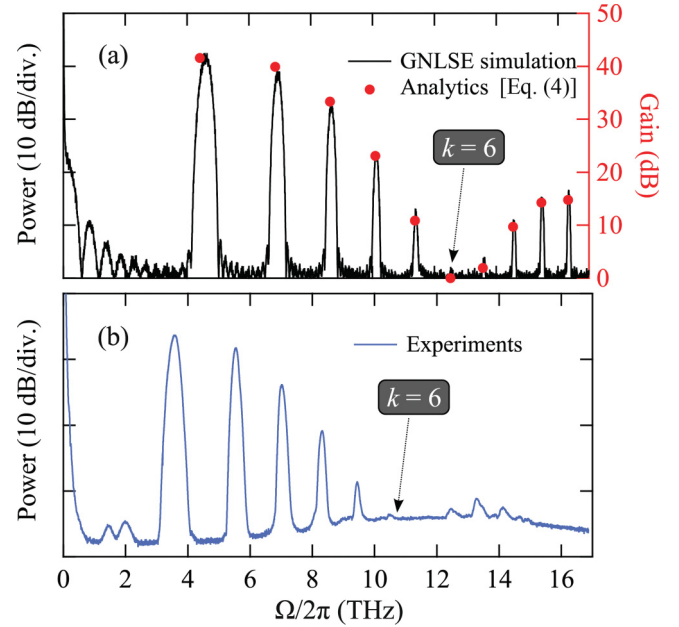


FIG. 5. (Color online) Illustration of the cancellation of the  $k = 6$  spectral component. (a) Maximal gain obtained from Eq. (7) (circles, right axis) and output spectrum simulated with the GNLSE (solid line, left axis), for  $\bar{\beta}_2 = 5.8 \times 10^{-28}$  s<sup>2</sup>/m and  $P_p = 13$  W. (b) Corresponding experiments performed in DOF2 for a pump wavelength of 1067.5 nm and pump power of 24 W.

canceled. Experiments performed in DOF2 by tuning the pump wavelength to 1067.5 nm (which is close to the required  $\bar{\beta}_2$  value of  $5.8 \times 10^{-28}$  s<sup>2</sup>/m) are displayed in Fig. 5(b).

The overall shape of the experimental spectrum nicely matches the one obtained from theory and this measurement also confirms the cancellation of the sixth peak. In all experiments presented in this section, the pump power was the only adjustable parameter. It had to be increased up to 24 W to observe the expected behaviors, which is higher than the power of 13 W used in simulations and in the model. This discrepancy in pump power is reasonable given the uncertainty in the evaluation of fiber properties (attenuation, dispersion, and nonlinearity) and in the pump laser parameters (repetition rate, pulse duration, and measurement of average power).

#### B. Maximization of a single spectral component

In order to further illustrate the possibility of tailoring the multi-peak MI spectrum, we use Eq. (7) to find a configuration in which the  $k = 1$  sideband is maximized, i.e., it experiences a much higher gain than any other sideband. In this case, we simply need to find a  $\bar{\beta}_2$  value (and thus a value of the  $\eta$  parameter), experimentally a pump wavelength, that maximizes the  $J_1$  Bessel function. Figure 6(a) shows the gain calculated from Eq. (7) as circles, as well as the output spectrum obtained from numerical integration of the GNLSE for a  $\bar{\beta}_2$  value of  $3.87 \times 10^{-28}$  s<sup>2</sup>/m. These results are again in excellent agreement and indeed show that the first sidelobe is favored since it has a 25-dB gain higher than all others. Experiments were performed by accordingly tuning the pump wavelength to 1071.5 nm. The output spectrum plotted in Fig. 6(b) shows that the power of the first sidelobe is 22 dB

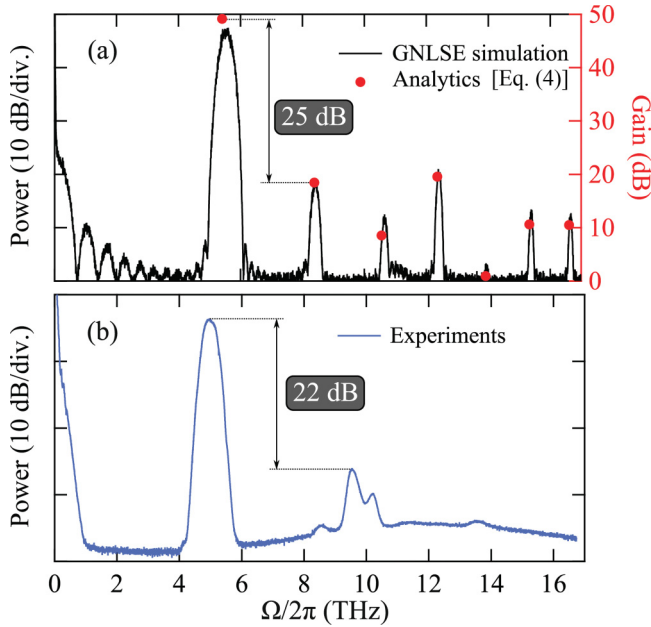


FIG. 6. (Color online) Illustration of the maximization of the  $k = 1$  spectral component. (a) Maximal gain obtained from Eq. (7) (circles, right axis) and simulated output spectrum (solid line, left axis), for  $\bar{\beta}_2 = 3.87 \times 10^{-28} \text{ s}^2/\text{m}$  and  $P_p = 13 \text{ W}$ . (b) Corresponding experiments performed in DOF2 for a pump wavelength of 1071.5 nm and pump power of 24 W.

higher than other spectral components, in good agreement with theoretical predictions.

It is also worth noting that in this case, the argument of the  $J_1$  Bessel function has been chosen so that the gain value of the first sideband calculated from our model corresponds to exactly the maximum value of 0.582 for  $J_1$ . This means that the gain brought by the periodicity for this sideband approximately equals  $0.582 \times 2\gamma P_p$  according to Eq. (7). It is less than a factor of 2 lower than the maximal gain expected from a classical MI process in the anomalous dispersion region in uniform fibers (which would be approximately equal to  $2\gamma P_p$ ). This observation is all the more important given that no gain is

expected in the normal dispersion region in uniform fibers (neglecting higher-order dispersion terms and higher-order fiber modes).

Although the control of the overall MI spectrum shape requires a change of quasi-phase-matched frequencies, these examples demonstrate the possibility of harnessing the MI spectrum thanks to the periodic dispersion landscape. A simultaneous control of both the spectral shape and sideband frequencies would still be possible by simultaneously adjusting  $\bar{\beta}_2$  and  $\beta_2^A$ , which would, however, require manufacturing new fibers.

## VI. CONCLUSION

Following our experimental demonstration of MI in dispersion oscillating fibers [17], here we have investigated this process theoretically. Starting from the well-known truncated three-wave model, we have derived an approximate analytical expression to predict the local parametric gain. This simplified model gives good agreement with numerical simulations and experiments. It has also allowed us to interpret the MI process in terms of a quasi-phase-matching mechanism due to the periodic nature of the fiber dispersion landscape. We have also used this model to emphasize the possibility of tailoring the MI spectrum, which has been confirmed experimentally by the cancellation or maximization of chosen spectral components.

Dispersion oscillating photonic crystal fibers such as the ones reported here and in Ref. [17] pave the way for a range of linear and nonlinear guided wave optical processes due to the longitudinal periodic modulation of their waveguiding properties. They should find applications in, for example, wavelength conversion, parametric amplification, generation of ultrashort pulse trains, and soliton management.

## ACKNOWLEDGMENTS

This work was partly supported by the ANR (IMFINI project), the French Ministry of Higher Education and Research, the Nord-Pas de Calais Regional Council, and FEDER through the Contrat de Projets Etat Région and the Campus Intelligence Ambiante.

- [1] F. K. Abdullaev, S. A. Darmanyan, J. Garnier, and E. Wolf, *Prog. Opt.* **44**, 303 (2002).
- [2] J. Meier, G. I. Stegeman, D. N. Christodoulides, Y. Silberberg, R. Morandotti, H. Yang, G. Salamo, M. Sorel, and J. S. Aitchison, *Phys. Rev. Lett.* **92**, 163902 (2004).
- [3] M. Centurion, M. A. Porter, Y. Pu, P. G. Kevrekidis, D. J. Frantzeskakis, and D. Psaltis, *Phys. Rev. Lett.* **97**, 234101 (2006).
- [4] S. G. Murdoch, M. D. Thomson, R. Leonhardt, and J. D. Harvey, *Opt. Lett.* **22**, 682 (1997).
- [5] S. G. Murdoch, R. Leonhardt, J. D. Harvey, and T. A. B. Kennedy, *J. Opt. Soc. Am. B* **14**, 1816 (1997).
- [6] K. Kikuchi, C. Lorattanasane, F. Futami, and S. Kaneko, *Photon. Technol. Lett.* **7**, 1378 (1995).
- [7] K. Shiraki, T. Omae, and T. Horiguchi, *Optical Fiber Communication Conference*, OSA Technical Digest Series Vol. 2 (Optical Society of America, Washington, DC, 1998), pp. 396–397.
- [8] F. Matera, A. Mecozzi, M. Romagnoli, and M. Settembre, *Opt. Lett.* **18**, 1499 (1993).
- [9] N. J. Smith and N. J. Doran, *Opt. Lett.* **21**, 570 (1996).
- [10] J. C. Bronski and J. N. Kutz, *Opt. Lett.* **21**, 937 (1996).
- [11] F. Abdullaev, S. Darmanyan, A. Kobayakov, and F. Lederer, *Phys. Lett. A* **220**, 213 (1996).
- [12] P. Kaewplung, T. Angkaew, and K. Kikuchi, *J. Lightwave Technol.* **20**, 1895 (2002).
- [13] F. Consolandi, C. De Angelis, A. Capobianco, G. Nalesso, and A. Tonello, *Opt. Commun.* **208**, 309 (2002).

- [14] A. Kumar, A. Labruyere, and P. Tchofo Dinda, *Opt. Commun.* **219**, 221 (2003).
- [15] S. Ambomo, C. M. Ngabireng, P. T. Dinda, A. Labruyère, K. Porsezian, and B. Kalithasan, *J. Opt. Soc. Am. B* **25**, 425 (2008).
- [16] J. B. Driscoll, N. Ophir, R. R. Grote, J. I. Dadap, N. C. Panoiu, K. Bergman, and R. M. Osgood, *Opt. Express* **20**, 9227 (2012).
- [17] M. Droques, A. Kudlinski, G. Bouwmans, G. Martinelli, and A. Mussot, *Opt. Lett.* **37**, 4832 (2012).
- [18] A. Armaroli and F. Biancalana, *Opt. Express* **20**, 25096 (2012).
- [19] It is important to make a clear distinction between these MI sidebands and so-called Kelly sidebands, which have been experimentally observed in the early years of soliton fiber lasers [20,21]. These two processes are by nature different [8] since Kelly sidebands originate from the destabilization of solitons and subsequent emission of resonant dispersive waves in active fiber cavities [22,23], whereas the MI process investigated here is a four-photon mixing process and therefore has a parametric origin.
- [20] R. Davey, N. Langford, and A. Ferguson, *Electron. Lett.* **27**, 1257 (1991).
- [21] D. Richardson, R. Laming, D. Payne, V. Matsas, and M. Phillips, *Electron. Lett.* **27**, 1451 (1991).
- [22] S. Kelly, *Electron. Lett.* **28**, 806 (1992).
- [23] N. Smith, K. Blow, and I. Andonovic, *J. Lightwave Technol.* **10**, 1329 (1992).
- [24] E. A. Golovchenko and A. N. Pilipetskii, *J. Opt. Soc. Am. B* **11**, 92 (1994).
- [25] J. D. Harvey, R. Leonhardt, S. Coen, G. K. L. Wong, J. C. Knight, W. J. Wadsworth, and P. S. J. Russell, *Opt. Lett.* **28**, 2225 (2003).
- [26] S. Trillo and S. Wabnitz, *Opt. Lett.* **16**, 986 (1991).
- [27] K. Inoue and T. Mukai, *Opt. Lett.* **26**, 10 (2001).
- [28] G. Van Simaëys, P. Emplit, and M. Haelterman, *J. Opt. Soc. Am. B* **19**, 477 (2002).
- [29] This is due to the fact that the nonuniform nonlinear phase-mismatched term  $\cos[\theta(\Omega, z)]$  in Eq. (3c) is neglected in this section.